THE JOURNAL OF PHYSICAL CHEMISTRY Letters

pubs.acs.org/JPCL Letter

Size-Dependent Hot Carrier Dynamics in Perovskite Nanocrystals Revealed by Two-Dimensional Electronic Spectroscopy

Buyang Yu,[§] Lan Chen,[§] Zhengkang Qu,[§] Chunfeng Zhang,* Zhengyuan Qin, Xiaoyong Wang, and Min Xiao*

Cite This: *J. Phys. Chem. Lett.* 2021, 12, 238−244 Read Online

ACCESS | Metrics & More | Article Recommendations | Supporting Information

ABSTRACT: The lifetimes of hot carriers have been predicted to be prolonged in small nanocrystals with an inter-level spacing larger than phonon energy. Nevertheless, whether such a phonon bottleneck is present in perovskite semiconductor nanocrystals remains highly controversial. Here we report compelling evidence of a phonon bottleneck in $CsPbI_3$ nanocrystals with marked size-dependent relaxation of hot carriers by using broadband two-dimensional electronic spectroscopy (2DES). By combining high resolutions in both the time (<10 fs) and excitation energy domains, 2DES allows the clear disentanglement of the thermalization and cooling processes. The lifetime is over doubled for hot carriers when the average edge length of the nanocrystals decreases from 8.2 nm down to 4.6 nm. The confirmation of the phonon bottleneck effect suggests the feasibility of controlling hot carrier dynamics in perovskite semiconductors with nanocrystal size for potential applications of hot carrier devices.

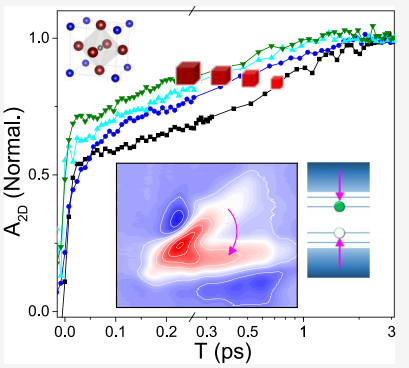

Hot carriers are generated in semiconductors above bandgap excitations. The excess energy dissipation of hot carriers is a major loss channel in conventional solar cells.[1] Hot carrier devices have been proposed to address this issue by harvesting hot carriers prior to carrier cooling, which, however, is limited by the short lifetimes of hot carriers in most semiconductors.[2−6] Recently, the emergent lead halide family of perovskite semiconductors has been regarded as a promising candidate for hot carrier applications. Possibly due to the carrier screening effect,[7−10] the hot carriers in such material systems have been found to be long-lived and can transport over 200 nm.[11]

Hot carrier dynamics is highly non-equilibrium, with multiple processes entangled on different temporal stages,[7] including the initial carrier thermalization before establishing the quasi-equilibrium of photoexcited carriers due to the carrier−carrier interaction (<100 fs), the hot carrier cooling due to the carrier−phonon interaction (<1 ps), and the lattice equilibrium due to the phonon−phonon interaction (1−10 ps). The lifetimes of hot carriers in perovskite semiconductors can be prolonged in nanocrystal structures owing to the quantum confinement. As the nanocrystal size decreases, the increased energy spacing between the discrete excitonic states will require the emission of multiple phonons, which may dramatically slow down the loss of excess energy of the hot carriers, known as the phonon bottleneck effect.[12−15] However, it is highly controversial whether such a phonon bottleneck is present in perovskite semiconductor nanocrystals, since very divergent size dependences of hot carrier dynamics have been reported in the literature. Sum et al.[14] and Butkus et al.[16] observed the phonon bottleneck effect by showing that the cooling of hot carriers slows down with decreasing sizes of $MAPbBr_3$ and $CsPbBr_3$ nanocrystals, respectively. On the other hand, Li et al.[17,18] observed a contrary size dependence in $CsPbBr_3$ and $FAPbBr_3$ nanocrystals, while Diroll et al.[19] and Cong et al.[20] reported no significant size dependence of hot carrier cooling in $CsPbBr_3$, $FAPbBr_3$, and $CsPbI_3$ nanocrystals. The divergent results in those previous studies have been ascribed to nanocrystal samples with diverse surface states[19] and the effects caused by high fluence excitation.[17] In addition, the measured lifetime parameter of hot carrier cooling is found to be dependent on the excess energy of pump photons.[21−25] Due to the Fourier transformation limit of the pump pulse, it is challenging to achieve satisfactory time and energy resolutions simultaneously to disentangle thermalization and cooling processes of hot carriers using conventional transient absorption (TA) spectroscopy. Consequently, the carrier thermalization and cooling processes are convoluted together in most available studies with the temporal resolution of 100 fs or longer, which possibly underestimates the size effect on hot carrier dynamics in perovskite nanocrystals.

Broadband two-dimensional electronic spectroscopy (2DES) can address the above issue by probing the nonlinear

Received: November 9, 2020
Accepted: December 10, 2020

https://dx.doi.org/10.1021/acs.jpclett.0c03350
J. Phys. Chem. Lett. 2021, 12, 238−244

optical signal induced by three sequence pulses,[26−28] which has been successfully applied to investigate the fine excitonic states, line shape dynamics, and biexciton interactions in perovskite nanostructures.[8,29−31] The excitation energy resolution is determined by the time interval between the first two pulses, and the time resolution in population delay is primarily limited by the pulse duration. In this work, we investigate hot carrier dynamics in $CsPbI_3$ nanocrystals with different sizes using 2DES with temporal resolution <10 fs. 2DES allows us to distinguish the thermalization (~20 fs) and cooling (260−800 fs) processes of hot carriers on the time domain. The measured lifetime parameter of hot carrier cooling is found to be dependent on the excess energy, the excitation fluence, and the sample size. With decreasing the average edge length of nanocrystals from 8.2 to 4.6 nm, the lifetime of hot carrier cooling under weak excitation becomes more than doubled. The experimental results strongly support the presence of the phonon bottleneck effect in strongly confined perovskite nanocrystals which can find potential applications in hot carrier devices.

To investigate the quantum confinement effect on hot carrier dynamics, we synthesized $CsPbI_3$ nanocrystals with different sizes following the literature procedure (details can be found in the Supporting Information).[32,33] Figure 1a,b shows the size-dependent absorption/photoluminescence (PL) spectra and transmission electron microscopy (TEM) images of

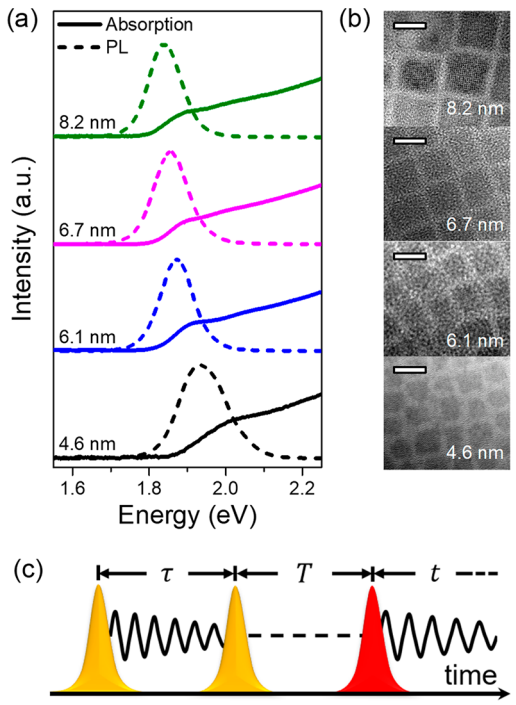

Figure 1. (a) Absorption (solid lines) and photoluminescence (PL; dashed lines) spectra of $CsPbI_3$ nanocrystals with different sizes. (b) Transmission electron microscopy (TEM) images of $CsPbI_3$ nanocrystals corresponding to the samples in (a) showing different sizes (scale bar, 10 nm). (c) Schematic diagram of the pulse sequence in 2DES measurements. Delays between the three incident pulses and the signal are denoted as τ, T, and t, respectively. 2DES has both excitation energy resolution (determined by τ-scan time) and temporal resolution (determined by pulse duration), so ultrafast processes under different excitation energies can be studied simultaneously.

$CsPbI_3$ nanocrystals. With decreasing nanocrystal size, the absorption/PL spectra show a significant blue shift due to the quantum confinement effect. The average sizes of nanocrystal samples used in the experiment are in the range between 4.6 and 8.2 nm, which are smaller than the exciton Bohr diameter of $CsPbI_3$ (~12 nm).[34]

We monitor the hot carrier dynamics using 2DES in a phase-stabilized pump−probe configuration as reported earlier[35] (details can be found in the Supporting Information). For absorptive 2D spectra using the pulse sequence shown in Figure 1, presented in this study, the excitation energy resolution is enabled by Fourier transformation of the signal in the time interval between the first two incident pulses (τ). The probe energy resolution, i.e., the Fourier transformation of the time interval between the third incident pulse and the signal, is directly achieved by a spectrometer. The temporal resolution in population delay (T) corresponding to the time delay of TA spectroscopy is set by the time delay between the second and third pulses. Using the ultrashort pulses generated by the non-collinear optical amplifiers, the overall temporal resolution of our setup is better than 10 fs in population delay (Figure S1). The pump fluence is ~5 $\mu J/cm^2$, corresponding to an average excitation density of ~0.2 electron−hole pair per nanocrystal, unless otherwise specified. In the weak pump intensity regime, 2DES signal is dominated by the third-order nonlinear optical response, as confirmed by a power-dependent measurement (Figure S2). The beams are linearly polarized in a parallel configuration. The data were recorded at room temperature.

Figure 2a shows the typical 2DES spectra recorded from a solution sample of $CsPbI_3$ nanocrystals with average size of 8.2 nm. The absorptive 2D data display the correlation between the electronic transitions resonant to the excitation and emission photon energies. The initial optical excitation is manifested with the positive signal along the diagonal, which is contributed by the ground-state bleaching and stimulated emission. The off-diagonal negative signals are possibly related to the excited-state absorption (ESA) of optical transitions to higher excited states or photoinduced stark effect.[36−39]

The hot carrier dynamics is manifested as the temporal evolution of the 2D signal with excitation energy significantly above the band gap value. Figure 2b shows the dynamics of 2D signals probed at different energies, with excitation excess energy of ΔE = 0.15 eV. The signal probed at the diagonal point (marked as A) represents the population occupied at the highly excited states. The signal probed in resonance with the excitonic energy (marked as B) is the bleaching signal induced by carriers relaxed to the band edge states. In addition, there is an ESA feature for hot carriers with probe energy below bandgap (marked as C). The temporal evolutions of these signals represent the dynamics of photoexcited hot carriers. In addition to the component with a characteristic lifetime on the time scale of 100 fs, the evolution within 100 fs accounts for a large proportion of the signal. The curves can be reproduced by considering two exponential components with lifetime parameters of ~20 and ~260 fs, respectively. The faster component is possibly caused by the carrier thermalization process to establish the quasi-equilibrium of photoexcited carriers as commonly assigned in TA studies[7,40] and/or the coherent many-body effects as uncovered in GaAs quantum wells.[41−44] Under weak excitation in nanocrystals, carrier thermalization may be triggered by the scattering between electrons and holes.[14] In comparison with the bulk values,[26]

https://dx.doi.org/10.1021/acs.jpclett.0c03350
J. Phys. Chem. Lett. 2021, 12, 238−244

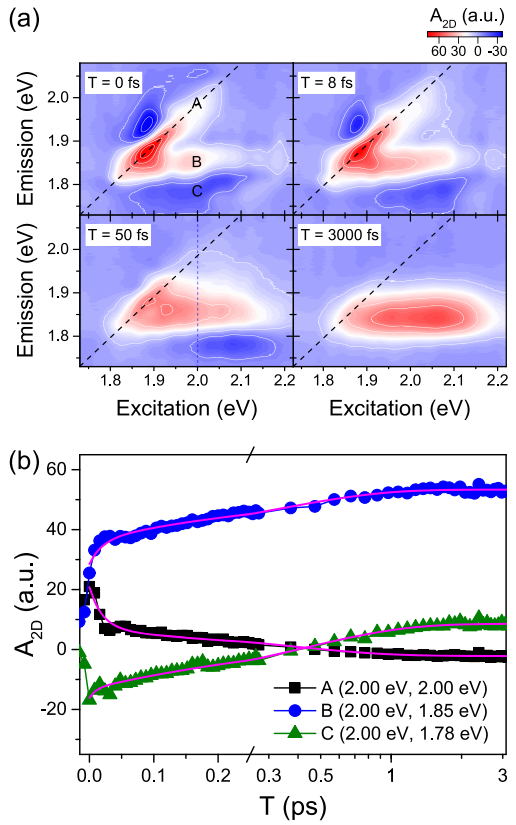

Figure 2. (a) Absorptive 2DES spectra recorded at representative population delays of T = 0, 8, 50, and 3000 fs. The diagonal is indicated with the dashed lines. (b) Temporal dynamics of 2DES signal probed at excitation excess energy of ΔE = 0.15 eV and different emission energies marked as A, B, and C in panel (a). The curves exhibit two-stage dynamics which can be reproduced by a biexponential function with lifetime parameters of ∼20 and ∼260 fs (pink lines), respectively. The data were recorded from the sample with an average size of 8.2 nm and an excitation fluence of ∼5 μJ cm^{-2}.

the lifetime parameter of carrier thermalization is faster, which is possibly related to the enhanced Coulomb scattering in nanocrystals. The slower component can be naturally ascribed to the cooling process of hot carriers with longitudinal-optical (LO) phonon emission.

To gain more insights into the two components, we analyze the sliced spectra at different population delays, as labeled in Figure 2a. Figure 3a,b highlights the sliced spectra with population delays <100 and >100 fs, respectively. The thermalization and cooling processes are both essential for the loss of excess energy of hot carriers. One marked difference between the two processes is the population redistribution behavior (Figure 3c). For carrier thermalization, the carriers may be scattered into higher energy levels due to carrier−carrier scattering (Figure S3). As expected for hot carrier thermalization, the early-stage spectral features (<100 fs) show broadening to higher and lower energy sides (Figure 3a).[26,40] For the carrier cooling process, the carriers relax to lower energy levels with LO phonon emission. With population delay, as shown in Figure 3b, the high-energy tail in the spectral profile gradually changes due to the net emission of LO phonons in the Fröhlich carrier−phonon scattering process, as analyzed by the hot-carrier temperature model (Figure 4c, black solid line, details can be found in the Supporting Information).[40,45,46] These results verify the experimental isolation of the thermalization and cooling processes of hot carriers by 2DES.

Pump fluence may significantly modify the cooling dynamics due to the Auger heating effect[22] and the density-dependent carrier−LO phonon scattering rate.[47] With the excitation density increasing, the Auger effect causes a much broader energy distribution of hot carriers. The phonon emission during the excess energy loss of hot carrier cooling results in a highly non-equilibrium population of LO phonons. As limited by LO phonon decay, the scattering rate between carriers and LO phonons decreases with increasing carrier density, which is often referred to as a hot phonon bottleneck.[46,48,49] These effects are observed in the excitation-density-dependent 2D measurements (Figures S4−S6). Figure 4 compares the dynamics of 2D signal probed under pump fluences of 5 and 50 $\mu J/cm^2$. In comparison with the thermalization process, the carrier cooling process slows down and becomes more prominent in the dynamics when the excitation density increases (Figure 4a). Notably, the effect of high excitation density is different for excitation of different excess energies (Figure 4b). The fluence dependence is more distinct in terms of hot-carrier temperature as analyzed with the model (Figure 4c). Upon high-fluence excitation, the temperature decays much more slowly due to the Auger heating and the hot phonon bottleneck. Thus, it is critical to exclude the high fluence effect and distinguish the thermalization and cooling processes in order to accurately evaluate the intrinsic rate of hot carrier cooling.

Next, we analyze the 2DES data recorded from nanocrystal samples with different sizes under weak pump excitation (Figure 5 and Figure S9). Figure 5a shows the dynamics of the 2D signal of the different samples probed on resonance with the excitonic transitions but with the same excess energy. The cooling process of hot carriers exhibits a marked size-dependent behavior. The size-dependent lifetime parameters of the hot carrier cooling process recorded with different excess energies are plotted in Figure 5b. Consistent with previous results, the relaxation time of hot carriers increases with increasing excess excitation energy.[21−24] When the nanocrystal size decreases, the slower cooling component of hot carriers becomes more important (Figure 5a). The lifetime becomes more than doubled with decreasing nanocrystal size from 8.2 to 4.6 nm (Figure 5b). These results provide clear evidence for the size-dependent phonon bottleneck effect in strongly confined perovskite nanocrystals, where multi-phonon processes are involved due to the larger gap between the excitonic states during the cooling of hot carriers in smaller nanocrystals. In this regime, the energy loss rate depends on the excess energy of the pump photon, especially in small nanocrystals (Figure S10). The loss rate increases with increasing excess energy, which is also a manifestation of the size-dependent phonon bottleneck effect.

In CdSe nanocrystals, the phonon bottleneck effect was reported to be absent. This phenomenon has been ascribed to the Auger-type electron-to-hole transfer mechanism, because the energy spacing between hole levels is much smaller due to the larger effective mass of the hole.[50−53] The effective masses of electron and hole are comparable in $CsPbI_3$ nanocrystals,[34] ensuring the observation of the size-dependent phonon bottleneck.

We now try to reconcile the diversely distributed results reported in the literature. The experimental data suggest that

https://dx.doi.org/10.1021/acs.jpclett.0c03350
J. Phys. Chem. Lett. 2021, 12, 238−244

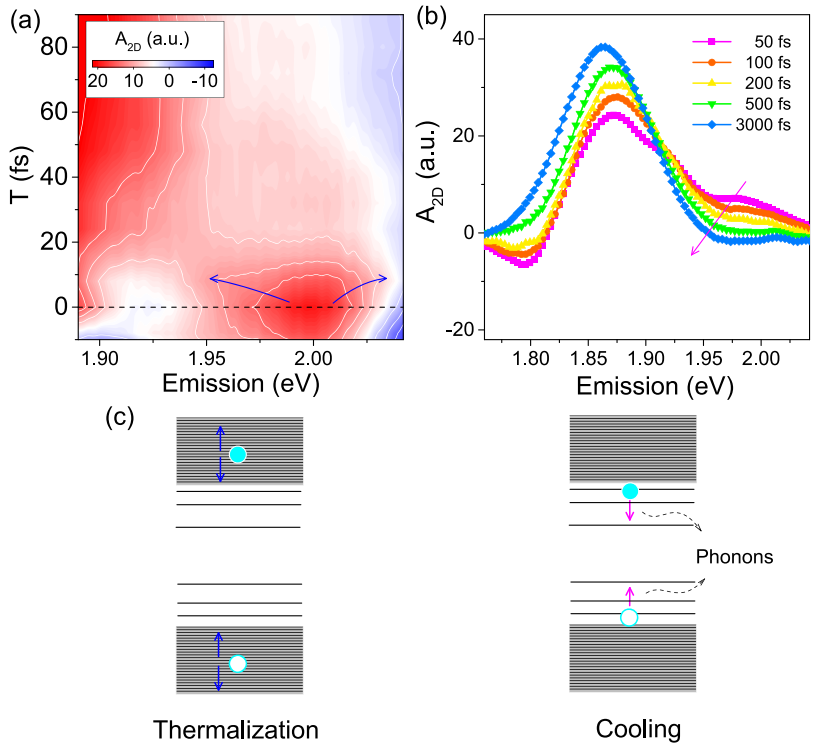

Figure 3. Spectral characteristics of hot carrier thermalization and cooling. (a) Contour plot of emission spectra at early stage (<100 fs) extracted from 2DES data. Due to the thermalization process, the spectral feature shows broadening to higher and lower energy sides. The data are obtained from 2D spectra sliced as marked in Figure 2a at different population delays. (b) Emission spectra extracted from 2DES data at different population delays (T). The excitation energy is selected at 2.00 eV. The data were recorded from the nanocrystal sample with an average size of 6.7 nm. (c) Schematic diagrams of the processes of hot carrier thermalization and cooling in perovskite semiconductor nanocrystals. The thermalization process is mainly induced by carrier−carrier scattering, and the cooling process is induced by carrier−phonon scattering.

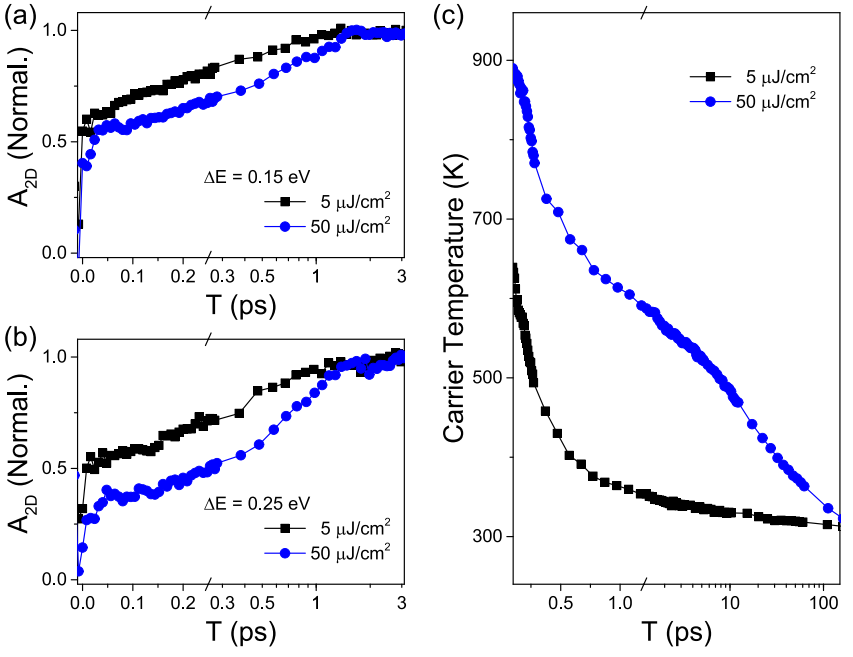

Figure 4. Pump-fluence-dependent hot carrier dynamics. Normalized time-resolved traces of 2D signals probed at the band edge with pump excess energy ΔE = (a) 0.15 and (b) 0.25 eV with fluences of 5 and 50 μJ cm^{-2}, respectively. (c) The dynamics of hot-carrier temperature derived by the model (Supporting Information) with pump fluences of 5 and 50 μJ cm^{-2}. The data were recorded from the nanocrystal sample with an average size of 6.7 nm.

high temporal resolution is probably necessary to accurately evaluate the lifetime parameters for hot carrier relaxation processes. In the dynamics probed at the band-edge states, the amplitude of the fast component (<100 fs) is more than half the magnitude of the total bleached signal. The convolution of the thermalization and cooling processes of hot carriers may

https://dx.doi.org/10.1021/acs.jpclett.0c03350
J. Phys. Chem. Lett. 2021, 12, 238−244

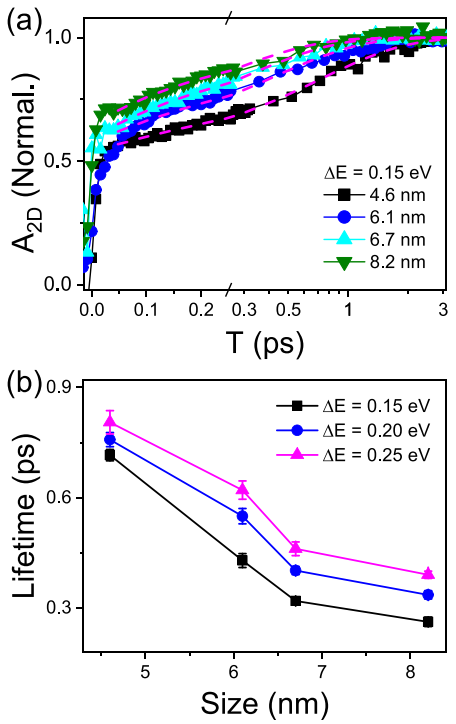

Figure 5. (a) Normalized time-resolved traces of 2D signal probed at the band edge from $CsPbI_3$ nanocrystals of different sizes with excess energy ΔE = 0.15 eV. The excitation fluence is set at 5 μJ cm^{-2}. The dashed line shows the exponential fitting of hot carrier cooling. (b) Size-dependent lifetime parameters for hot carrier dynamics. The cooling process slows down with decreasing nanocrystal size as a signature of the phonon bottleneck effect.

significantly underestimate the lifetime for the cooling process, especially in the strongly confined nanocrystals. In comparison to $CsPbI_3$ nanocrystals, the Bohr diameter of $MAPbBr_3$ nanocrystals (4 nm)[54] is much smaller. With sizes in the intermediate and weak confinement regions, the measurements with a slower temporal resolution can plausibly uncover the size dependence of lifetime parameters of hot carrier cooling despite the convolution of thermalization and cooling processes in the previous study on $MAPbBr_3$ nanocrystals.[14] In strongly confined nanocrystals, the lifetime parameter is much less sensitive to the excess energy of pump photons (i.e., excitation wavelength), which is consistent with previous observations with small $CsPbBr_3$ nanocrystals.[17] Such a behavior is also a consequence of a phonon bottleneck due to the large gap between the lowest-lying excitonic states in strongly confined perovskite nanocrystals. Moreover, in the strong confinement region, the wave function of photoexcited carriers may partially distribute over the surface of the nanocrystal, resulting in non-adiabatic hot carrier relaxation relevant to the ligands, like that in CdSe nanocrystals.[55−57] In this case, the size dependence of hot carrier relaxation time may change.

In summary, we have studied the size dependences of hot carrier dynamics in $CsPbI_3$ nanocrystals using 2DES measurements. By combining the high resolutions in the temporal and excitation energy domains of 2DES, we have been able to disentangle the thermalization and cooling processes in the time domain. Under weak excitation, the lifetime of the hot carrier cooling process increases dramatically when the size of nanocrystals is reduced down to the strongly confined regime, verifying the presence of a phonon bottleneck effect in perovskite nanocrystals. Our finding has settled a highly debated controversial issue in perovskite semiconductor nanocrystals, implying promising potential applications using perovskite nanocrystals for hot carrier optoelectronic devices.

■ ASSOCIATED CONTENT

Supporting Information

The Supporting Information is available free of charge at https://pubs.acs.org/doi/10.1021/acs.jpclett.0c03350.

Details of sample preparations and 2DES measurements, power-dependent TA measurements, analysis of hot carrier energy distribution and loss rate, and Figures S1−S10, showing fringe-resolved autocorrelation (FRAC) trace of the pump pulse, contour plot of emission spectra of different excitation fluence at early stage, emission spectra of different excitation fluence, absorptive 2DES spectra of the other three samples, time-resolved traces of 2D signal probed at the band edge, and energy loss rate of the four samples (PDF)

■ AUTHOR INFORMATION

Corresponding Authors

Chunfeng Zhang − *National Laboratory of Solid State Microstructures, School of Physics, and Collaborative Innovation Center for Advanced Microstructures, Nanjing University, Nanjing 210093, China;* orcid.org/0000-0001-9030-5606; Email: cfzhang@nju.edu.cn

Min Xiao − *National Laboratory of Solid State Microstructures, School of Physics, and Collaborative Innovation Center for Advanced Microstructures, Nanjing University, Nanjing 210093, China; Department of Physics, University of Arkansas, Fayetteville, Arkansas 72701, United States*; Email: mxiao@uark.edu

Authors

Buyang Yu − *National Laboratory of Solid State Microstructures, School of Physics, and Collaborative Innovation Center for Advanced Microstructures, Nanjing University, Nanjing 210093, China*

Lan Chen − *National Laboratory of Solid State Microstructures, School of Physics, and Collaborative Innovation Center for Advanced Microstructures, Nanjing University, Nanjing 210093, China*

Zhengkang Qu − *National Laboratory of Solid State Microstructures, School of Physics, and Collaborative Innovation Center for Advanced Microstructures, Nanjing University, Nanjing 210093, China*

Zhengyuan Qin − *National Laboratory of Solid State Microstructures, School of Physics, and Collaborative Innovation Center for Advanced Microstructures, Nanjing University, Nanjing 210093, China*

Xiaoyong Wang − *National Laboratory of Solid State Microstructures, School of Physics, and Collaborative Innovation Center for Advanced Microstructures, Nanjing University, Nanjing 210093, China;* orcid.org/0000-0003-1147-0051

Complete contact information is available at: https://pubs.acs.org/10.1021/acs.jpclett.0c03350

Author Contributions

[§]B.Y., L.C., and Z.Q. contributed equally.

https://dx.doi.org/10.1021/acs.jpclett.0c03350
J. Phys. Chem. Lett. 2021, 12, 238−244

Notes

The authors declare no competing financial interest.

■ ACKNOWLEDGMENTS

This work was supported by the National Key R&D Program of China (Nos. 2018YFA0209101 and 2017YFA0303703), the National Natural Science Foundation of China (Nos. 21922302, 21873047, 91850105, and 91833305), the Priority Academic Program Development of Jiangsu Higher Education Institutions (PAPD), and the Fundamental Research Funds for the Central Universities. The authors thank Dr. Xuewei Wu for technical assistance.

■ REFERENCES

(1) Shockley, W.; Queisser, H. J. Detailed balance limit of efficiency of p−n junction solar cells. *J. Appl. Phys.* **1961**, *32* (3), 510−519.
(2) Green, M. A. Third generation photovoltaics: Ultra-high conversion efficiency at low cost. *Prog. Photovoltaics* **2001**, *9* (2), 123−135.
(3) Tisdale, W. A.; Williams, K. J.; Timp, B. A.; Norris, D. J.; Aydil, E. S.; Zhu, X.-Y. Hot-electron transfer from semiconductor nanocrystals. *Science* **2010**, *328* (5985), 1543−1547.
(4) Nelson, C. A.; Monahan, N. R.; Zhu, X. Y. Exceeding the Shockley−Queisser limit in solar energy conversion. *Energy Environ. Sci.* **2013**, *6* (12), 3508.
(5) Wang, G.; Liao, L. P.; Elseman, A. M.; Yao, Y. Q.; Lin, C. Y.; Hu, W.; Liu, D. B.; Xu, C. Y.; Zhou, G. D.; Li, P.; Chen, L. J.; Han, J. J.; De Yang, X.; Wu, R.; Rao, X.; Song, Q. L. An internally photoemitted hot carrier solar cell based on organic-inorganic perovskite. *Nano Energy* **2020**, *68* (1), 104383.
(6) Lim, S. S.; Giovanni, D.; Zhang, Q.; Solanki, A.; Jamaludin, N. F.; Lim, J. W. M.; Mathews, N.; Mhaisalkar, S.; Pshenichnikov, M. S.; Sum, T. C. Hot carrier extraction in $CH_3NH_3PbI_3$ unveiled by pump-push-probe spectroscopy. *Sci. Adv.* **2019**, *5* (11), eaax3620.
(7) Joshi, P. P.; Maehrlein, S. F.; Zhu, X. Dynamic screening and slow cooling of hot carriers in lead halide perovskites. *Adv. Mater.* **2019**, *31* (47), 1803054.
(8) Seiler, H.; Palato, S.; Sonnichsen, C.; Baker, H.; Socie, E.; Strandell, D. P.; Kambhampati, P. Two-dimensional electronic spectroscopy reveals liquid-like lineshape dynamics in $CsPbI_3$ perovskite nanocrystals. *Nat. Commun.* **2019**, *10* (1), 4962.
(9) Zhu, H.; Miyata, K.; Fu, Y.; Wang, J.; Joshi, P. P.; Niesner, D.; Williams, K. W.; Jin, S.; Zhu, X.-Y. Screening in crystalline liquids protects energetic carriers in hybrid perovskites. *Science* **2016**, *353* (6306), 1409−1413.
(10) Puppin, M.; Polishchuk, S.; Colonna, N.; Crepaldi, A.; Dirin, D. N.; Nazarenko, O.; De Gennaro, R.; Gatti, G.; Roth, S.; Barillot, T.; Poletto, L.; Xian, R. P.; Rettig, L.; Wolf, M.; Ernstorfer, R.; Kovalenko, M. V.; Marzari, N.; Grioni, M.; Chergui, M. Evidence of large polarons in photoemission band mapping of the perovskite semiconductor $CsPbBr_3$. *Phys. Rev. Lett.* **2020**, *124* (20), 206402.
(11) Guo, Z.; Wan, Y.; Yang, M.; Snaider, J.; Zhu, K.; Huang, L. Long-range hot-carrier transport in hybrid perovskites visualized by ultrafast microscopy. *Science* **2017**, *356* (6333), 59−62.
(12) Benisty, H.; Sotomayor-Torres, C. M.; Weisbuch, C. Intrinsic mechanism for the poor luminescence properties of quantum-box systems. *Phys. Rev. B: Condens. Matter Mater. Phys.* **1991**, *44* (19), 10945−10948.
(13) Nozik, A. J. Spectroscopy and hot electron relaxation dynamics in semiconductor quantum wells and quantum dots. *Annu. Rev. Phys. Chem.* **2001**, *52* (1), 193−231.
(14) Li, M.; Bhaumik, S.; Goh, T. W.; Kumar, M. S.; Yantara, N.; Gratzel, M.; Mhaisalkar, S.; Mathews, N.; Sum, T. C. Slow cooling and highly efficient extraction of hot carriers in colloidal perovskite nanocrystals. *Nat. Commun.* **2017**, *8* (1), 14350.
(15) Forde, A.; Inerbaev, T.; Hobbie, E. K.; Kilin, D. S. Excited-state dynamics of a $CsPbBr_3$ nanocrystal terminated with binary ligands: Sparse density of states with giant spin-orbit coupling suppresses carrier cooling. *J. Am. Chem. Soc.* **2019**, *141* (10), 4388−4397.
(16) Butkus, J.; Vashishtha, P.; Chen, K.; Gallaher, J. K.; Prasad, S. K. K.; Metin, D. Z.; Laufersky, G.; Gaston, N.; Halpert, J. E.; Hodgkiss, J. M. The evolution of quantum confinement in $CsPbBr_3$ perovskite nanocrystals. *Chem. Mater.* **2017**, *29* (8), 3644−3652.
(17) Li, Y.; Lai, R.; Luo, X.; Liu, X.; Ding, T.; Lu, X.; Wu, K. On the absence of a phonon bottleneck in strongly confined $cspbbr_3$ perovskite nanocrystals. *Chem. Sci.* **2019**, *10* (23), 5983−5989.
(18) Li, Y.; Ding, T.; Luo, X.; Tian, Y.; Lu, X.; Wu, K. Synthesis and spectroscopy of monodispersed, quantum-confined $FAbBr_3$ perovskite nanocrystals. *Chem. Mater.* **2020**, *32* (1), 549−556.
(19) Diroll, B. T.; Schaller, R. D. Intraband cooling in all-inorganic and hybrid organic−inorganic perovskite nanocrystals. *Adv. Funct. Mater.* **2019**, *29* (37), 1901725.
(20) Cong, M.; Yang, B.; Chen, J.; Hong, F.; Yang, S.; Deng, W.; Han, K. Carrier multiplication and hot-carrier cooling dynamics in quantum-confined $CsPbI_3$ perovskite nanocrystals. *J. Phys. Chem. Lett.* **2020**, *11* (5), 1921−1926.
(21) Yang, Y.; Ostrowski, D. P.; France, R. M.; Zhu, K.; van de Lagemaat, J.; Luther, J. M.; Beard, M. C. Observation of a hot-phonon bottleneck in lead-iodide perovskites. *Nat. Photonics* **2016**, *10* (1), 53−59.
(22) Fu, J.; Xu, Q.; Han, G.; Wu, B.; Huan, C. H. A.; Leek, M. L.; Sum, T. C. Hot carrier cooling mechanisms in halide perovskites. *Nat. Commun.* **2017**, *8* (1), 1300.
(23) Mondal, N.; Samanta, A. Complete ultrafast charge carrier dynamics in photo-excited all-inorganic perovskite nanocrystals ($CsPbX_3$). *Nanoscale* **2017**, *9* (5), 1878−1885.
(24) Chen, J.; Messing, M. E.; Zheng, K.; Pullerits, T. Cation-dependent hot carrier cooling in halide perovskite nanocrystals. *J. Am. Chem. Soc.* **2019**, *141* (8), 3532−3540.
(25) Righetto, M.; Lim, S. S.; Giovanni, D.; Lim, J. W. M.; Zhang, Q.; Ramesh, S.; Tay, Y. K. E.; Sum, T. C. Hot carriers perspective on the nature of traps in perovskites. *Nat. Commun.* **2020**, *11* (1), 2712.
(26) Richter, J. M.; Branchi, F.; Valduga de Almeida Camargo, F.; Zhao, B.; Friend, R. H.; Cerullo, G.; Deschler, F. Ultrafast carrier thermalization in lead iodide perovskite probed with two-dimensional electronic spectroscopy. *Nat. Commun.* **2017**, *8* (1), 376.
(27) Smallwood, C. L.; Cundiff, S. T. Multidimensional coherent spectroscopy of semiconductors. *Laser Photonics Rev.* **2018**, *12* (12), 1800171.
(28) Moody, G.; Cundiff, S. T. Advances in multi-dimensional coherent spectroscopy of semiconductor nanostructures. *Adv. Phys.* **2017**, *2* (3), 641−674.
(29) Liu, A.; Nagamine, G.; Bonato, L. G.; Almeida, D. B.; Zagonel, L. F.; Nogueira, A. F.; Padilha, L. A.; Cundiff, S. Towards enginnering intrinsic linewidths and line-broadening in perovskite nanoplatelets. *arXiv Preprint* **2020**, arXiv:2011.02816 [physics.optics].
(30) Liu, A.; Almeida, D. B.; Bonato, L. G.; Nagamine, G.; Zagonel, L. F.; Nogueira, A. F.; Padilha, L. A.; Cundiff, S. Partially-bright triple excitons in perovskite nanocrystals. *arXiv Preprint* **2020**, arXiv:2002.08349 [cond-mat.mtrl-sci].
(31) Huang, X.; Chen, L.; Zhang, C.; Qin, Z.; Yu, B.; Wang, X.; Xiao, M. Inhomogeneous biexciton binding in perovskite semiconductor nanocrystals measured with two-dimensional spectroscopy. *J. Phys. Chem. Lett.* **2020**, *11* (23), 10173−10181.
(32) Swarnkar, A.; Marshall, A. R.; Sanehira, E. M.; Chernomordik, B. D.; Moore, D. T.; Christians, J. A.; Chakrabarti, T.; Luther, J. M. Quantum dot−induced phase stabilization of α-$CsPbI_3$ perovskite for high-efficiency photovoltaics. *Science* **2016**, *354* (6308), 92−95.
(33) Yao, J. S.; Ge, J.; Wang, K. H.; Zhang, G.; Zhu, B. S.; Chen, C.; Zhang, Q.; Luo, Y.; Yu, S. H.; Yao, H. B. Few-nanometer-sized alpha-$CsPbI_3$ quantum dots enabled by strontium substitution and iodide passivation for efficient red-light emitting diodes. *J. Am. Chem. Soc.* **2019**, *141* (5), 2069−2079.
(34) Protesescu, L.; Yakunin, S.; Bodnarchuk, M. I.; Krieg, F.; Caputo, R.; Hendon, C. H.; Yang, R. X.; Walsh, A.; Kovalenko, M. V. Nanocrystals of cesium lead halide perovskites ($CsPbX_3$,X = Cl, Br,

https://dx.doi.org/10.1021/acs.jpclett.0c03350
J. Phys. Chem. Lett. 2021, 12, 238−244

and I): Novel optoelectronic materials showing bright emission with wide color gamut. *Nano Lett.* **2015**, *15* (6), 3692−3696.
(35) Zhu, W.; Wang, R.; Zhang, C.; Wang, G.; Liu, Y.; Zhao, W.; Dai, X.; Wang, X.; Cerullo, G.; Cundiff, S.; Xiao, M. Broadband two-dimensional electronic spectroscopy in an actively phase stabilized pump-probe configuration. *Opt. Express* **2017**, *25* (18), 21115−21126.
(36) Yumoto, G.; Tahara, H.; Kawawaki, T.; Saruyama, M.; Sato, R.; Teranishi, T.; Kanemitsu, Y. Hot biexciton effect on optical gain in $CsPbI_3$ perovskite nanocrystals. *J. Phys. Chem. Lett.* **2018**, *9* (9), 2222−2228.
(37) Xu, Y.; Chen, Q.; Zhang, C.; Wang, R.; Wu, H.; Zhang, X.; Xing, G.; Yu, W. W.; Wang, X.; Zhang, Y.; Xiao, M. Two-photon-pumped perovskite semiconductor nanocrystal lasers. *J. Am. Chem. Soc.* **2016**, *138* (11), 3761−3768.
(38) Zhao, W.; Qin, Z.; Zhang, C.; Wang, G.; Huang, X.; Li, B.; Dai, X.; Xiao, M. Optical gain from biexcitons in $CsPbBr_3$ nanocrystals revealed by two-dimensional electronic spectroscopy. *J. Phys. Chem. Lett.* **2019**, *10* (6), 1251−1258.
(39) Zhao, W.; Qin, Z.; Zhang, C.; Wang, G.; Dai, X.; Xiao, M. Coherent exciton-phonon coupling in perovskite semiconductor nanocrystals studied by two-dimensional electronic spectroscopy. *Appl. Phys. Lett.* **2019**, *115* (24), 243101.
(40) Li, M.; Fu, J.; Xu, Q.; Sum, T. C. Slow hot-carrier cooling in halide perovskites: Prospects for hot-carrier solar cells. *Adv. Mater.* **2019**, *31* (47), 1802486.
(41) Borca, C. N.; Zhang, T. H.; Li, X. Q.; Cundiff, S. T. Optical two-dimensional fourier transform spectroscopy of semiconductors. *Chem. Phys. Lett.* **2005**, *416* (4−6), 311−315.
(42) Li, X. Q.; Zhang, T. H.; Borca, C. N.; Cundiff, S. T. Many-body interactions in semiconductors probed by optical two-dimensional Fourier transform spectroscopy. *Phys. Rev. Lett.* **2006**, *96* (5), 057406.
(43) Turner, D. B.; Wen, P.; Arias, D. H.; Nelson, K. A.; Li, H.; Moody, G.; Siemens, M. E.; Cundiff, S. T. Persistent exciton-type many-body interactions in GaAs quantum wells measured using two-dimensional optical spectroscopy. *Phys. Rev. B: Condens. Matter Mater. Phys.* **2012**, *85* (20), 201303.
(44) Zhang, T.; Kuznetsova, I.; Meier, T.; Li, X.; Mirin, R. P.; Thomas, P.; Cundiff, S. T. Polarization-dependent optical 2D Fourier transform spectroscopy of semiconductors. *Proc. Natl. Acad. Sci. U. S. A.* **2007**, *104* (36), 14227−14232.
(45) Price, M. B.; Butkus, J.; Jellicoe, T. C.; Sadhanala, A.; Briane, A.; Halpert, J. E.; Broch, K.; Hodgkiss, J. M.; Friend, R. H.; Deschler, F. Hot-carrier cooling and photoinduced refractive index changes in organic-inorganic lead halide perovskites. *Nat. Commun.* **2015**, *6* (1), 8420.
(46) Yang, J.; Wen, X.; Xia, H.; Sheng, R.; Ma, Q.; Kim, J.; Tapping, P.; Harada, T.; Kee, T. W.; Huang, F.; Cheng, Y. B.; Green, M.; Ho-Baillie, A.; Huang, S.; Shrestha, S.; Patterson, R.; Conibeer, G. Acoustic-optical phonon up-conversion and hot-phonon bottleneck in lead-halide perovskites. *Nat. Commun.* **2017**, *8* (1), 14120.
(47) Papagiorgis, P.; Protesescu, L.; Kovalenko, M. V.; Othonos, A.; Itskos, G. Long-lived hot carriers in formamidinium lead iodide nanocrystals. *J. Phys. Chem. C* **2017**, *121* (22), 12434−12440.
(48) Mondal, A.; Aneesh, J.; Kumar Ravi, V.; Sharma, R.; Mir, W. J.; Beard, M. C.; Nag, A.; Adarsh, K. V. Ultrafast exciton many-body interactions and hot-phonon bottleneck in colloidal cesium lead halide perovskite nanocrystals. *Phys. Rev. B: Condens. Matter Mater. Phys.* **2018**, *98* (11), 115418.
(49) Joshi, R. P.; Ferry, D. K. Hot-phonon effects and interband relaxation processes in photoexcited GaAs quantum wells. *Phys. Rev. B: Condens. Matter Mater. Phys.* **1989**, *39* (2), 1180−1187.
(50) Klimov, V. I.; McBranch, D. W. Femtosecond 1p-to-1s electron relaxation in strongly confined semiconductor nanocrystals. *Phys. Rev. Lett.* **1998**, *80* (18), 4028−4031.
(51) Klimov, V. I.; McBranch, D.; Leatherdale, C.; Bawendi, M. Electron and hole relaxation pathways in semiconductor quantum dots. *Phys. Rev. B: Condens. Matter Mater. Phys.* **1999**, *60* (19), 13740−13749.
(52) Schaller, R. D.; Pietryga, J. M.; Goupalov, S. V.; Petruska, M. A.; Ivanov, S. A.; Klimov, V. I. Breaking the phonon bottleneck in semiconductor nanocrystals via multiphonon emission induced by intrinsic nonadiabatic interactions. *Phys. Rev. Lett.* **2005**, *95* (19), 196401.
(53) Cooney, R. R.; Sewall, S. L.; Anderson, K. E. H.; Dias, E. A.; Kambhampati, P. Breaking the phonon bottleneck for holes in semiconductor quantum dots. *Phys. Rev. Lett.* **2007**, *98* (17), 177403.
(54) Tanaka, K.; Takahashi, T.; Ban, T.; Kondo, T.; Uchida, K.; Miura, N. Comparative study on the excitons in lead-halide-based perovskite-type crystals $CH_3NH_3PbBr_3$ $CH_3NH_3PbI_3$. *Solid State Commun.* **2003**, *127* (9−10), 619−623.
(55) Kambhampati, P. Unraveling the structure and dynamics of excitons in semiconductor quantum dots. *Acc. Chem. Res.* **2011**, *44* (1), 1−13.
(56) Kambhampati, P. Hot exciton relaxation dynamics in semiconductor quantum dots: Radiationless transitions on the nanoscale. *J. Phys. Chem. C* **2011**, *115* (45), 22089−22109.
(57) Cooney, R. R.; Sewall, S. L.; Dias, E. A.; Sagar, D. M.; Anderson, K. E. H.; Kambhampati, P. Unified picture of electron and hole relaxation pathways in semiconductor quantum dots. *Phys. Rev. B: Condens. Matter Mater. Phys.* **2007**, *75* (24), 245311.

https://dx.doi.org/10.1021/acs.jpclett.0c03350
J. Phys. Chem. Lett. 2021, 12, 238−244